Journal of Biomedical Optics

BiomedicalOptics.SPIEDigitalLibrary.org

First step toward translation of thermophotonic lock-in imaging to dentistry as an early caries detection technology

Ashkan Ojaghi
Artur Parkhimchyk
Nima Tabatabaei

SPIE.

Ashkan Ojaghi, Artur Parkhimchyk, Nima Tabatabaei, "First step toward translation of thermophotonic lock-in imaging to dentistry as an early caries detection technology," *J. Biomed. Opt.* **21**(9), 096003 (2016), doi: 10.1117/1.JBO.21.9.096003.

First step toward translation of thermophotonic lock-in imaging to dentistry as an early caries detection technology

Ashkan Ojaghi, Artur Parkhimchyk, and Nima Tabatabaei*
York University, Department of Mechanical Engineering, 4700 Keele Street, Toronto, Ontario M3J 1P3, Canada

Abstract. Early detection of the most prevalent oral disease worldwide, i.e., dental caries, still remains as one of the major challenges in dentistry. The current dental standard of care relies on caries detection methods, such as visual inspection and x-ray radiography, which lack the sufficient specificity and sensitivity to detect caries at early stages of formation when they can be healed. We report on the feasibility of early caries detection in a clinically and commercially viable thermophotonic imaging system. The system incorporates intensity-modulated laser light along with a low-cost long-wavelength infrared (LWIR; 8 to 14 μm) camera, providing diagnostic contrast based on the enhanced light absorption of early caries. The LWIR camera is highly suitable for integration into clinical platforms because of its low weight and cost. In addition, through theoretical modeling, we show that LWIR detection enhances the diagnostic contrast due to the minimal LWIR transmittance of enamel and suppression of the masking effect of the direct thermal Planck emission. Diagnostic performance of the system and its detection threshold are experimentally evaluated by monitoring the inception and progression of artificially induced occlusal and smooth surface caries. The results are suggestive of the suitability of the developed LWIR system for detecting early dental caries. [DOI: 10.1117/1.JBO.21.9.096003]

Keywords: early dental caries; long-wavelength infrared; thermophotonic lock-in imaging; early detection; artificial demineralization.

Paper 160383PR received Jun. 8, 2016; accepted for publication Aug. 23, 2016; published online Sep. 8, 2016.

1 Introduction

Development of sensitive dental diagnostic modalities capable of detecting early caries has been the focus of a number of studies over the past years.[1–9] Dental caries is an oral infection known as the most prevalent dental disease among children and adult populations worldwide and is the leading cause of tooth loss.[2,8] The inception of tooth decay in caries starts with minute amounts of mineral loss (i.e., demineralization) from the enamel surface as a result of the decomposition of hydroxyapatite crystals in the acidic environment of dental plaques.[10] If a prolonged acidic environment is maintained, early caries progresses deeper into the dentine forming a cavity which necessitates costly and labor-intensive surgical interventions. However, if dental caries is detected early enough, its progression can be stopped (i.e., arrested caries) or even reversed (i.e., healed/remineralized) through preventive actions, such as oral hygiene counseling or fluoride therapy.[11] Nevertheless, existing clinical caries inspection methods, such as x-ray radiography and visual/tactile assessment, lack sufficient sensitivity and specificity to detect early caries.[12] As such, a number of new technologies are currently under development to address the need for sensitive and reliable detection of caries at early stages of formation. Among these technologies, optical diagnostic methods have shown great potential as they utilize the intrinsic difference between optical properties (e.g., absorption or scattering) of the sound and demineralized tissues as the source of diagnostic contrast. Fiber-optic transillumination (FOTI)[1] is one such imaging method, which uses high intensity white light for detecting caries. However, significant scattering of light in the visible spectrum as well as the masking effect of background signal originating from the healthy tissue surrounding the malignancy leads to relatively poor sensitivity and inconsistent results for FOTI.[1] Working on similar physical principles, near-infrared (NIR) transmission/reflectance methods use NIR light instead of visible light to gain deeper penetration into dental hard tissues as a result of reduced scattering and absorption of enamel in the NIR region. However, poor detection specificity to early demineralization has been reported for these technologies mainly due to reliance of the diagnostic contrast on enhanced light scattering within the caries sites, which can effectively be masked by the light scattering of the surrounding intact tissues and the anisotropic structure of dentin.[2,3,13]

Optical coherence tomography (OCT) is another promising modality capable of imaging the tissue microstructure within the caries lesions. OCT works based on coherent collection of NIR backscattered light from an illuminated focal volume within the tissue and the analysis of the light intensity as it interferes with a reference light beam.[8] The intensity of the interference is dependent upon the degree of scattering caused by structural changes in the dental tissue.[14] Fried et al.[8] have demonstrated the application of a modified OCT system capable of producing polarization-sensitive OCT images to monitor caries lesion progression *in vitro*. Although promising results have been reported from this study, due to the relatively slow imaging speed of the

*Address all correspondence to: Nima Tabatabaei, E-mail: nima.tabatabaei@lassonde.yorku.ca

1083-3668/2016/$25.00 © 2016 SPIE

OCT technology, only isolated cross-sectional (B-scan) images were reported rather than diagnostic images of the whole tooth. Several other studies have also been conducted to demonstrate the ability of OCT in detection of demineralization in enamel.[15] However, factors, such as formation of image artifacts as a result of the interfering effect of intact tissues surrounding the malignancies with the backscattered light from caries, loss of coherence for deep zone imaging due to high light scattering, low imaging speed for inspection of entire tooth surface, and high equipment cost limit the clinical adaptation of dental OCT.[16]

Another category of optical diagnostic methodologies is known as energy conversion technologies, which operate based on transformation of optical energy to other energy forms. Quantitative light-induced fluorescence (QLF) is one such method, which uses light-to-fluorescence conversion and the decrease in fluorescence transmission due to increased scattering from demineralized spots as a source of contrast. In QLF, fluorescence is caused by the excitation of fluorophores contained within the enamel–dentin junction using visible light. Although QLF is capable of detecting early carious lesions,[4] its sensitivity to the masking effects of surface stains as well as the need for extensive operator training hinder the applicability of this technique in most real-life clinical scenarios.[15] DIAGNODent is another caries detection device based on fluorescence, which uses red light illumination to excite the bacterial porphyrins found in dental caries. The major downside of this method is the fact that it measures bacterial activity rather than structural changes in enamel. In addition, the fluorescence emission from caries-related bacteria can be masked by emission from other florescence emitting substances present in the oral cavity, such as stains, plaque, food, fissure sealants, composite resin materials, and even the tooth itself, which can result in false-positive readings.[15]

Thermophotonic lock-in (TPLI) imaging is an alternative imaging modality which has recently been proposed for early dental caries detection.[9] This hybrid caries detection technology belongs to the group of energy conversion methodologies, where the excitation and detection channels are separated (i.e., optical excitation and thermal detection). In this imaging modality, the crosstalk between the two channels occurs at caries sites as a result of enhanced local optical absorption within caries lesions.[17]

TPLI is based on the detection of the thermal IR (Planck) radiation from caries and uses diffusive thermal waves as markers to gather information about subsurface caries. In this method, a low-power, continuous, and intensity-modulated light source is utilized to generate a thermal wave field inside the tooth and the subsequent IR emission of the thermal wave field is captured using an IR camera.[9] The role of lock-in demodulation is to only evaluate the alternating (ac) part of the detected signal, which carries information from subsurface inhomogeneities.[9] That is, subsurface defects alter the local centroid of the thermal wave field, leading to a phase delay as well as a change in the amplitude of the ac radiometric detected signal by the IR camera. As such, lock-in demodulation of the thermophotonic signals lead to calculation of phase and amplitude images with respect to the reference signal (i.e., optical excitation modulation signal).[9]

One of the first studies incorporating lock-in thermography for medical diagnosis was conducted by John and Salerno[5] and John et al.[6] They examined the ground section of a resin-embedded extracted human tooth using modulated optical excitation and lock-in thermography. However, the result of their study was limited only to estimation of the relative thermal thicknesses of dental samples and no diagnostic study was carried out. In a more recent study, Tabatabaei et al.[9,18] used thermophotonic imaging (TPI) for detection of early stages of demineralization in dental tissues using a research-grade mid-wavelength infrared (MWIR) camera. The study demonstrated the great potential of TPLI for detecting early dental caries and its diagnostic outperformance over another emerging technology (i.e., polarized Raman spectroscopy);[19] however, the IR camera used in this study was an expensive (~USD $80k) research-grade camera with integrated cryogenic cooling system not suitable for commercialization and clinical translation to dentistry. As such, this paper takes the first step in translation of TPLI technology into dentistry by studying the diagnostic performance of an economically viable long-wavelength infrared (LWIR) thermophotonic lock-in imaging system for detecting early dental caries.

Recent advances in the field of microelectronics have enabled the design and manufacturing of LWIR and uncooled microbolometer detector arrays, which no longer require integrated cryogenic cooling systems, leading to a reduction in the size, weight, and cost of the IR cameras. In addition to affordability and small form factor, the use of LWIR over MWIR detectors for interrogation of teeth at near ambient temperatures is advantageous as the peak of the black body radiation falls in the LWIR band at room temperature, providing considerably higher photon flux to the detector and consequently, a better detection signal-to-noise ratio. Furthermore, from the thermal-wave science point of view, radiometric interrogation of enamel in the LWIR band is advantageous as the direct Plank emission (radiative heat transfer) from subsurface regions is effectively suppressed due to the minimal optical transmittance of enamel (enamel transmittance: MWIR = 75%, LWIR = 7%[13]), allowing the registration of pure conductive thermal waves by the camera, which carry the diagnostic information.[20]

Despite the widespread implementation of LWIR detectors in nondestructive evaluation of industrial materials,[21–24] to this day, active LWIR thermography has not been used for diagnostic imaging of biomedical samples. As such, the overarching aim of the present study, which is partially based on our previously published conference proceedings paper,[25] as the first biomedical active thermography research in the LWIR band is to integrate the low-cost (~USD $8k) LWIR technology in a lock-in thermography system to make the first step toward translation of the existing dental MWIR technology[9] to dentistry as a clinically and commercially viable device.

2 Theoretical Modeling of Caries Detection in the Mid-Infrared and Long-Wavelength Infrared Bands

The light–matter interaction in turbid media (e.g., dental hard tissues) is governed by strongly coupled diffuse-photon-density and thermal-wave processes.[26] In the case of dental caries, the enhanced local optical scattering and absorption at caries results in the generation of strong subsurface thermal-wave sources, contributing to the IR detector signal radiometrically in the form of the following depth-integrated formula[26]

$$S(l;t) \propto \bar{\mu}_{\mathrm{IR}} \int_0^l T(z,t)\exp(-\bar{\mu}_{\mathrm{IR}} z)\mathrm{d}z, \tag{1}$$

where $\bar{\mu}_{\mathrm{IR}}$, l, and $T(z,t)$ are the average IR absorption coefficient over the detection wavelength bandwidth (MWIR: 3 to 5 μm, LWIR: 8 to 14 μm), caries/absorber depth, and the induced thermal-wave field, respectively.

Equation (1) suggests that the radiometric signal registered by the IR detector gets contributions from the thermal-wave field in the form of an exponentially attenuated depth-integral, with $\bar{\mu}_{\mathrm{IR}}$ serving as the attenuation coefficient. Therefore, the spectral bandwidth of the detector (MWIR versus LWIR) plays an important role in the physical nature of the acquired IR signals. In the case of an MWIR TPLI system, the direct Plank emission (radiative heat transfer) from subsurface thermal sources (e.g., early caries) dominates the conductive thermal-wave contribution from the interrogation surface as a result of relatively low $\bar{\mu}_{\mathrm{IR}}$ (enamel transmittance: MWIR = 75%)[13] in this spectral region. Such dominant radiative contribution from subsurface thermal sources in the MWIR band is carried out at the speed of light (i.e., no delay), masking the desirable delayed conductive thermal-wave contribution required for generating diagnostic contrast in dental TPLI images. In contrast to the MWIR band, $\bar{\mu}_{\mathrm{IR}}$ is significantly large within the LWIR band (enamel transmittance: LWIR = 7%[13]), which effectively results in attenuation of the instantaneous radiative contribution from the subsurface thermal sources, allowing for reliable detection of delayed thermal-wave contributions emanating from the sample surface, which carry the desired diagnostic information.

To demonstrate the advantages of LWIR TPLI in detection of subsurface absorbers in turbid media, thermophotonic signals from thermal sources located at different depths are theoretically modeled and the LWIR TPLI and MWIR TPLI responses are compared. That is, the thermophotonic response (Planck radiation emission) of a turbid medium subjected to an amplitude-modulated optical excitation is calculated by solving the associated coupled diffuse-photon-density and thermal-wave field boundary value problem, as a simplified model of the real-life problem (i.e., dental caries detection). Subsequently, the response of black body absorbers (i.e., defects/early caries) located at different depths inside a turbid medium with known scattering and absorption coefficients (μ_{s} and μ_{a}, respectively) is analytically derived. The frequency-domain thermal-wave problem can be formulated [Eq. (2)] by considering a depth-dependent source term [i.e., attenuated energy fluence of a beam $I(z)$[20]] for the heat diffusion differential equation as well as a thermal source (e.g., early caries) at $z = L$ through the boundary condition

$$\begin{cases} \frac{\partial^2\theta(z;\omega)}{\partial z^2} - \sigma^2\theta(z;w) = -\frac{\mu_a}{k} I(z)F(\omega) \\ -k\frac{\partial\theta(z;\omega)}{\partial z}|_{z=0} = 0 = 0 \\ -k\frac{\partial\theta(z;\omega)}{\partial z}|_{z=l} = I(l)F(\omega) \\ \theta(z;\omega) = \Im\{T(z,t) - T_\infty\}, \end{cases} \tag{2}$$

where k, T_∞, and $F(\omega)$ are thermal conductivity, sample equilibrium temperature, and the spectrum of the applied optical excitation, respectively. $\Im$ denotes the Fourier transform operator and $\sigma = \sqrt{i\omega/\alpha}$ is the complex wavenumber, where ω and α are the laser modulation frequency and thermal diffusivity, respectively.

By solving the differential equation, the spectrum of radiometric signal can be calculated as

$$\begin{aligned} S_c(l;\omega) &\propto \bar{\mu}_{\mathrm{IR}} \int_0^l \theta(z,\omega)\exp(-\bar{\mu}_{\mathrm{IR}} z)\mathrm{d}z \\ &= \bar{\mu}_{\mathrm{IR}}\left[\frac{A}{\sigma - \bar{\mu}_{\mathrm{IR}}}\{\exp[(\sigma - \bar{\mu}_{\mathrm{IR}})l] - 1\}\right. \\ &\quad - \frac{B}{\sigma + \bar{\mu}_{\mathrm{IR}}}\{\exp[-(\sigma + \bar{\mu}_{\mathrm{IR}})l] - 1\} \\ &\quad - \frac{C}{\mu_{\mathrm{eff}} + \bar{\mu}_{\mathrm{IR}}}\{\exp[-(\mu_{\mathrm{eff}} + \bar{\mu}_{\mathrm{IR}})l] - 1\} \\ &\quad \left. - \frac{D}{\mu_t + \bar{\mu}_{\mathrm{IR}}}\{\exp[-(\mu_t + \bar{\mu}_{\mathrm{IR}})l] - 1\}\right], \end{aligned} \tag{3}$$

where $\mu_{\mathrm{eff}} = \sqrt{3\mu_a\mu_t}$, $\mu_t = \mu_a + \mu_s'$, $\mu_s' = \mu_s(1-g)$. g is the average cosine of the scattering angle. In this study, the absorption coefficient, scattering coefficient, thermal conductivity, and thermal diffusivity are chosen based on the properties of dental enamel to be 100 m^{-1}, 6000 m^{-1}, 0.9 $\mathrm{Wm}^{-1}\mathrm{k}^{-1}$, and 5×10^{-7} $\mathrm{m}^2\,\mathrm{s}^{-1}$, respectively.[17]

The radiometric signal is calculated for two extreme values of IR absorption coefficients, corresponding to the two detection spectral bands (i.e., 100 m^{-1} for MWIR and 50,000 m^{-1} LWIR) at three different absorber depths (100, 500, and 900 μm) at 2 Hz modulation frequency. The modeled lock-in amplitude values for absorbers located at 100, 500, and 900 μm below the interrogation surface for the MWIR and LWIR detection bands are shown in Figs. 1(a) and 1(b), respectively. The normalized amplitude values suggest that for MWIR detection (small $\bar{\mu}_{\mathrm{IR}}$), the amplitude of the signal exhibits poor sensitivity to absorber depth as a result of low absorption of direct thermal radiation by the medium and the consequent domination of the instantaneous direct Planck radiation over the delayed conductive thermal waves. On the other hand, in the case of LWIR detection (large $\bar{\mu}_{\mathrm{IR}}$), the amplitude difference at various depths (i.e., detection sensitivity) becomes considerable as the instantaneous Planck IR radiation is strongly absorbed by the medium surrounding the subsurface thermal sources, allowing for the proper detection of delayed conductive thermal waves.

The lock-in phase values for signals originated from absorbers at different depths are also modeled for both values of IR absorption coefficients. As depicted in Figs. 1(c) and 1(d), a similar behavior to the amplitude values is observed in the phase channel. At the MWIR detection band, the instantaneous contributions of the direct Planck emission from deep regions dominate the conductive thermal wave contributions. Consequently, there will be minimal contrast between defects located at different depths. On the contrary, the modeling results at the LWIR band show a substantial phase difference between the signals originating from absorbers at different depths. The phase values demonstrate such a trend due to the suppression of direct IR (Planck) emission, allowing only the thermal waves to conductively reach the surface of the tooth and contribute to the camera signal. The obtained results from theoretical modeling demonstrate that LWIR detection yields better diagnostic contrast in TPI of dental hard tissues than the existing caries detection technology in the MWIR band.

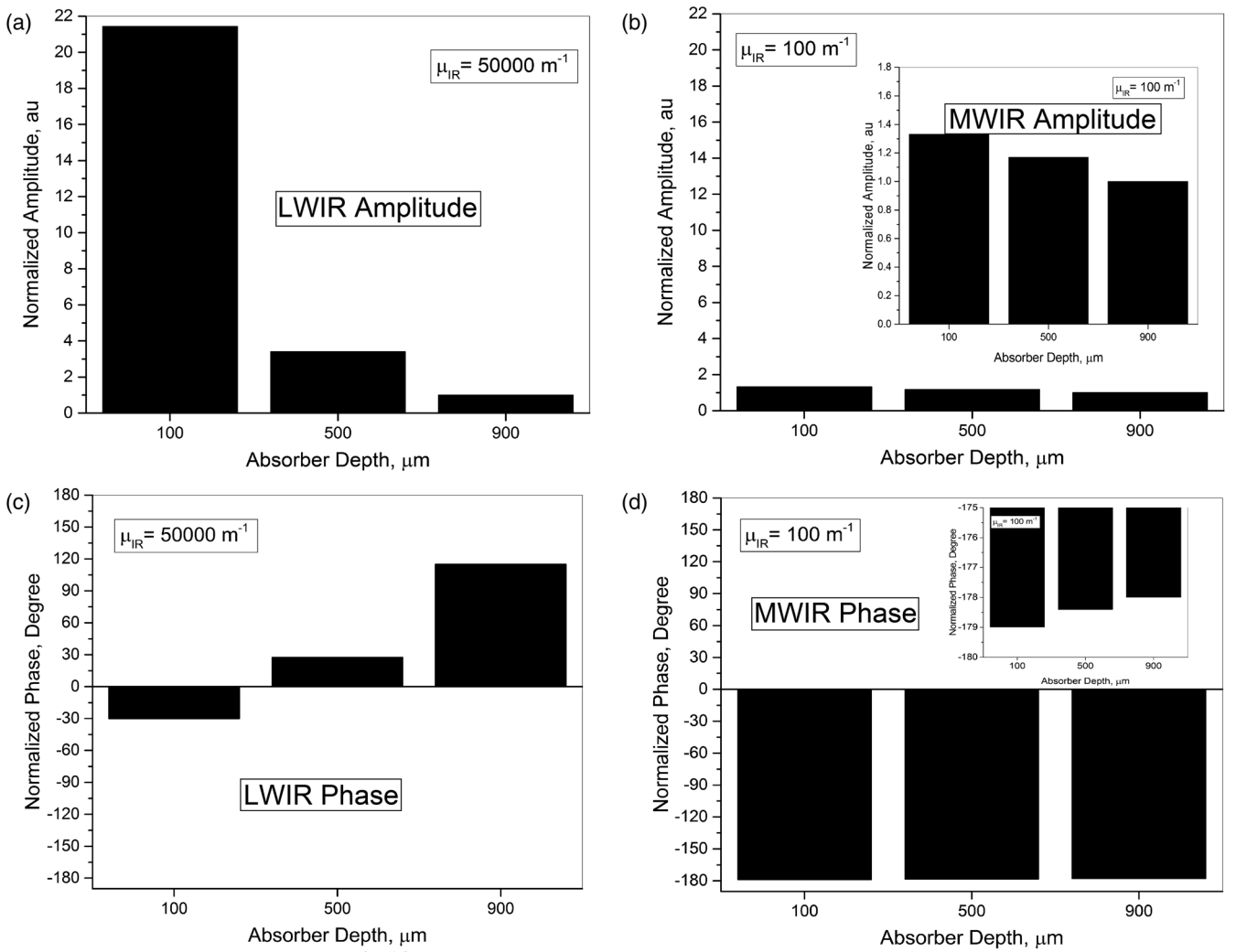

Fig. 1 Phase and amplitude of the theoretical radiometric signals calculated for MWIR and LWIR detection spectral bands for absorbers located at different depths: normalized amplitude values for (a) LWIR ($\bar{\mu}_{IR} = 50{,}000$ m^{-1}) and (b) MWIR ($\bar{\mu}_{IR} = 100$ m^{-1}) and normalized phase values for (c) LWIR ($\bar{\mu}_{IR} = 50{,}000$ m^{-1}) and (d) MWIR ($\bar{\mu}_{IR} = 100$ m^{-1}).

3 Materials and Methods

3.1 *Experimental Setup*

Figure 2(a) depicts a schematic of the LWIR TPLI system used in this study. The setup consists of a multimode fiber coupled (core diameter = 200 μm) continuous-wave NIR laser (808 nm; Jenoptik, Jena, Germany). A laser controller unit (Ostech, Berlin, Germany) is used to thermally stabilize the laser and to modulate its intensity. In order to have an illumination beam with uniform optical intensity over the interrogated area of the sample, a collimator (Thorlabs, Newton, New Jersey, F220SMA-780) in conjunction with an optical diffuser (Thorlabs, Newton, New Jersey, ED1-C20-MD) is used.

A low-cost LWIR camera (Xenics, Leuven, Belgium) with Cameralink communication protocol standard, spectral range of 8 to 14 μm, and maximum frame rate of 50 fps is focused on the surface of a LEGO-mounted sample. The sample is placed on a rotation stage mounted on a three-axis XYZ translation stage (precision 10 μm). An 18-mm focal-length objective lens (Xenics OPT-000179) along with a custom made extension tube is installed on the camera to obtain a magnification of unity (1) from the interrogated surface of the sample. LWIR camera frames are acquired by a frame grabber (Euresys, Angleur, Belgium, Grablink Full). A multifunctional data acquisition board (National Instruments, Austin, Texas, NI USB-6363 BNC) synchronously generates three analog signals: reference pulse train, in-phase, and quadrature reference signals. The laser controller modulates the intensity of the laser beam using the in-phase reference signal.

The lock-in demodulation algorithm [Fig. 2(b)] is implemented in a computer program, designed in the LabView environment, which captures the images at a specified frame rate and at the same time records the corresponding values of in-phase and quadrature signals as well as the reference pulse train status (high or low).The program captures an image sequence and finds the beginning of a modulation cycle using the pulse train information and uses the reference signal values to calculate the weighted average of an image sequence corresponding to an integer multiple of lock-in modulation period using the instantaneous readings of the two reference signals [Fig. 2(b)]. Subsequently, the weighted frames are summed to obtain the

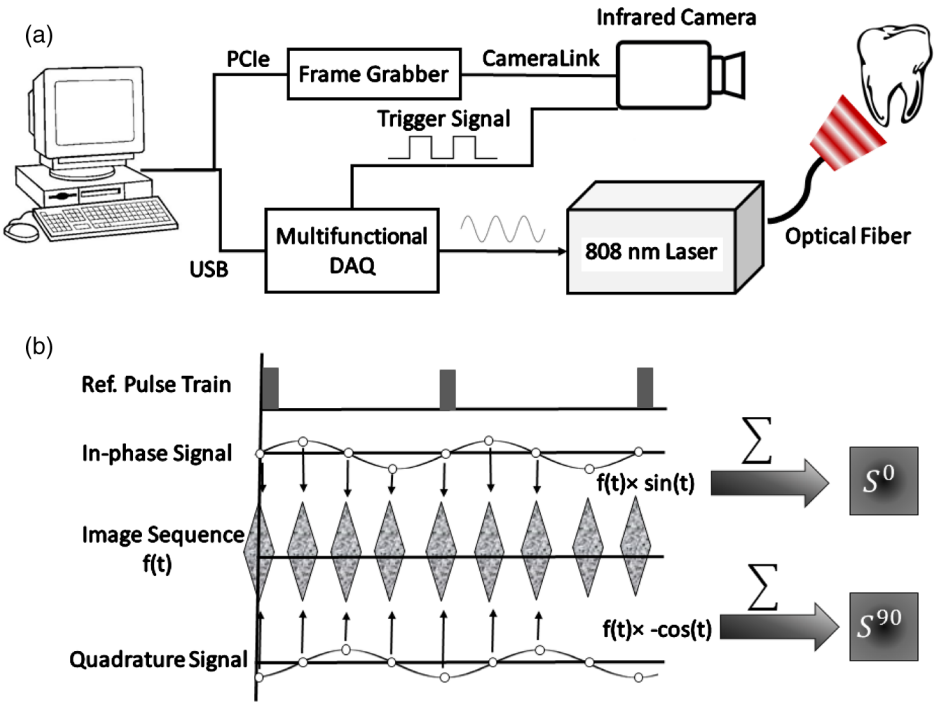

Fig. 2 (a) The experimental setup consisting of a NIR laser, an LWIR camera, a frame grabber, and a multifunctional DAQ device. (b) Signal processing algorithm.

low-pass filtered in-phase (S^0) and quadrature (S^{90}) images. The amplitude and phase images are then calculated by applying [Eq. (4)] to each pixel:

$$A = \sqrt{(S^0)^2 + (S^{90})^2} \quad \text{and} \quad \varphi = \arctan\left(\frac{S^{90}}{S^0}\right). \tag{4}$$

3.2 *Synchronous Undersampling*

One of the limitations of inexpensive IR cameras is the low frame rate (e.g., maximum of 50 Hz for the LWIR camera used in this study), limiting their ability to monitor high frequency phenomena. Theoretically, to retrieve the amplitude and phase information of signals, a minimum of $n = 4$ samples per modulation cycle are to be obtained;[27] however, oversampling of typically $n = 10$ is often employed in practice to achieve an acceptable signal to noise ratio. To overcome the acquisition speed limitation in our LWIR TPLI system, for modulation frequencies above 5 Hz, the LabView data acquisition program automatically runs a subroutine based on the synchronous undersampling algorithm in which the required "n" samples per modulation cycle are captured from "n" consecutive cycles instead of 1.[27] Using this method, the developed system can reliably interrogate dental samples at photothermal modulation frequencies of up to 1 kHz.

3.3 *Samples*

In this study, the diagnostic performance of the LWIR imaging system is evaluated through artificial demineralization of dental samples. Following the research ethics guidelines in place at York University, extracted human molars were obtained from local dental offices and those with no visible stains or white spot lesions were selected for the study. After preliminary visual inspection, the samples were cleaned and mounted on LEGO blocks using an epoxy adhesive. This allows the samples to be remounted in the same position in the experimental setup during repeated measurements.

3.4 *Controlled Demineralization Protocol*

A widely used lactic acid-based solution[9,19,28–32] was applied on dental samples to induce controlled demineralization. The solution was an acidified gel, consisting of 0.1 M lactic acid and 0.1 M NaOH, gelled to a thick consistency with the addition of 6% w/v hydroxyethylcellulose. The aim of controlled demineralization in the current study was to observe the contrast between demineralized and healthy areas during different stages of caries formation. To this end, a treatment protocol was followed in a time-dependent experiment in which the tooth surface was covered with an acid-resistant transparent nail polish except for a 2.5 mm (W) × 5 mm (H) rectangular window (i.e., treatment window). The demineralization on the window was carried out by submerging the sample in a test tube containing 20 ml of demineralizing gel. The treatment was repeated in 4 or 6 h as well as 2-day intervals for the detection threshold and controlled demineralization studies, respectively. After each treatment, the sample was removed from the gel, cleaned by rinsing under running water, and dried in air. Then the transparent nail polish was removed from the interrogated surface with nail polish remover and the sample was again rinsed and air dried before TPLI. In addition, a photograph of the sample was taken using a high magnification CCD camera at each demineralization step to monitor the appearance of the white spot lesion. After imaging, the sample was again covered with the transparent nail polish (except for the treatment window) and demineralized for an additional treatment interval in order to investigate the progression of demineralization. The treatment window of samples used in this study was

demineralized for up to 10 days and imaging was carried out on the untreated sample and after each treatment step. Several studies carried out using gold standard methods, such as transverse microradiography, have verified the ability of this demineralization protocol in producing a subsurface lesion in enamel with a sound surface layer (i.e., the characteristic mineral profile of early dental caries).[19,29–31,33]

4 Results and Discussion

To investigate the progression of demineralization into the enamel over time, a systematic normalization procedure[9] was employed to the TPI phase images to ensure that the sequence of images taken at various stages of demineralization is self-consistent as the optical and thermal properties of teeth slightly change over time. That is, for any given phase image, the pixel values were normalized by the average pixel value of an intact reference area [e.g., dashed reference area in Fig. 3(c)]. This normalization is the only modification made on the raw TPLI phase images. In this article, only thermophotonic phase images are presented as, in contrast to the amplitude images, phase images are intrinsically emissivity normalized,[18] which makes them insensitive to the variations in the optical power of the laser and/or surface conditions (e.g., stain) of the sample. Moreover, the excitation wavelength and detection spectral band are carefully selected, based on the existing literature, to avoid interference of biofilms[34–36] and stains[37–39] with TPI of early caries.

4.1 *Detection of Smooth Surface Caries*

The visual photograph of the sample before demineralization is depicted in Fig. 3(a). The dashed rectangle indicates the interrogated surface of the sample in our TPI system, whereas the solid rectangle shows the location of the treatment window. No dominant defect is visually observed in this sample. The TPLI phase image obtained at 2 Hz modulation frequency before application of artificial demineralization [Fig. 3(c)] also confirms this finding. As such, the sample was deemed to be reasonably healthy before application of the demineralization protocol. The visual photograph of the sample after application of demineralization for 10 days is shown in Fig. 3(b). To acquire the photographs, the samples are air-blown for 10 s and dried to simulate the condition under which the visual inspection of caries is typically carried out in clinic. Comparison of the two visual photographs, carried out by a dental practitioner blinded to the study, indicated no obvious sign of mineral loss (i.e., white spot lesion) within the treatment window even after 10 days of demineralization, suggesting the insensitivity of the conventional visual inspection method to detection of early demineralization. However, the presence of a lesion is clearly observed in the TPLI phase image of Fig. 3(d) taken after only 2 days of demineralization, confirming the ability of the LWIR TPLI system to identify early caries not detectable via visual inspection.

Figures 3(d)–3(h) show the phase images taken at 2, 4, 6, 8, and 10 days of treatment, respectively. It should be noted that the same contrast mapping has been applied to all images of Fig. 3 to ensure the validity of comparison between the images. Careful inspection of the image sequence obtained at different stages of demineralization reveals that as the treatment time increases, the caries lesion becomes more apparent while the intact areas in the images appear with a similar contrast. This monotonic increase in the average phase values is due to the substitution of hydroxyapatite crystals from close-to-surface enamel with microcavities leading to an increase in the demineralized lesion depth, which enhances local light scattering and absorption near the surface. As the demineralized region's thickness increases, the thermal-wave centroid shifts farther away from the surface, resulting in an increase in the phase lag between the optical excitation (i.e., reference signal) and the acquired IR response signal.

To further demonstrate the changes in phase values over various stages of demineralization progression, the average phase

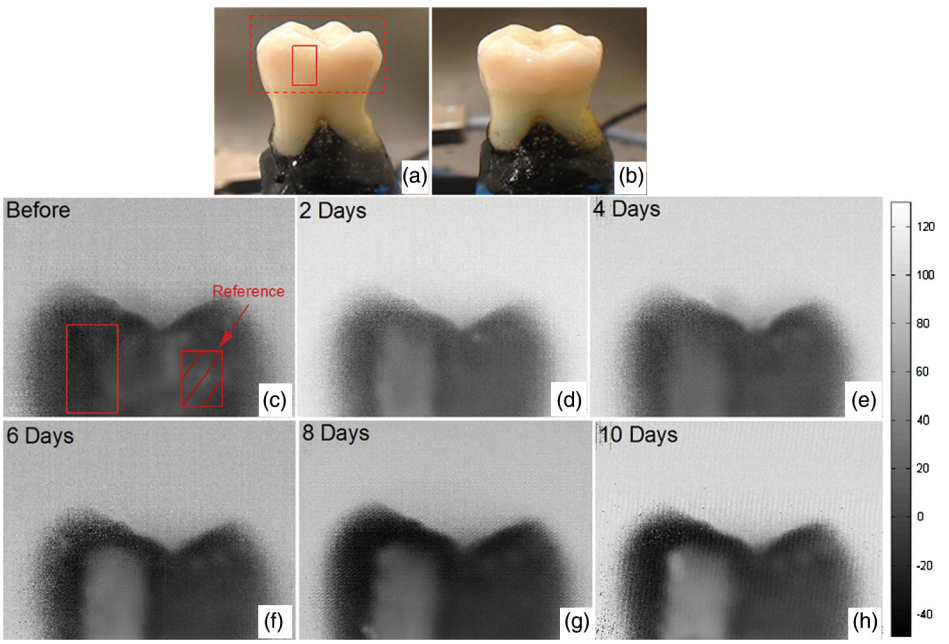

Fig. 3 Optical image of the smooth surface of extracted human molar (a) before demineralization and (b) after 10 days of demineralization on the treatment window. TPLI phase images of sample (c) before and after (d) 2, (e) 4, (f) 6, (g) 8, and (h) 10 days of treatment obtained at 2-Hz modulation frequency.

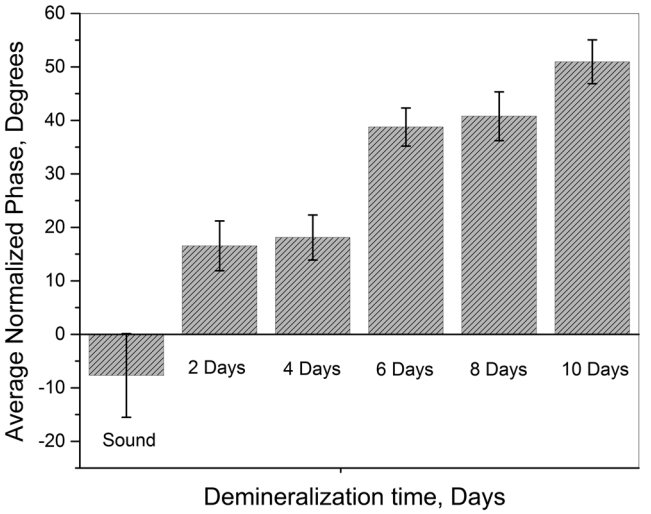

Fig. 4 Average phase values within the treatment window for samples at several demineralization stages.

values within the treatment window and the corresponding standard deviations are plotted in Fig. 4. The increasing trend in the contrast between treated and intact areas can be quantitatively validated by comparing the average phase values for the untreated, 2, 4, 8, and 10 days of treatment, which are found to be −7.69, 16.54, 18.12, 38.75, 40.77, and 50.95 deg, respectively. The increasing trend in phase values indicates the shift of the thermal-wave centroid away from the interrogated surface of enamel as more minerals are removed from the enamel. The obtained results demonstrate the ability of the developed low-cost LWIR TPLI system in detecting early smooth surface caries not detectable through visual inspection.

4.2 *Detection of Occlusal Caries*

Occlusal caries are the most prevalent type of dental caries, which can progress deep into the enamel and form a cavity. The significance of detection of early occlusal caries lies in the fact that this surface cannot directly be inspected through x-ray radiography. The reason for this limitation is that x-ray radiography works based on the transmission of radiation through the enamel and as such proper interrogation of occlusal surface requires the detector to be placed beneath the occlusal surface, which is not feasible in dental practice. However, TPLI operates in reflection mode and can thus directly interrogate the occlusal surface.

In order to test the ability of the developed low-cost TPI system to detect early occlusal caries, a 10-day demineralization procedure, similar to that applied to smooth surface of a tooth, is applied on a treatment window placed on the occlusal surface of a relatively healthy sample [shown in Figs. 5(a) and 5(c)]. Figure 5(b) shows a photograph of the sample after 10 days of treatment. No obvious indication of demineralization is observed in this image. On the contrary, the inception and progression of early occlusal caries is clearly evident in the TPLI phase images of Fig. 5. Figures 5(c)–5(h) exhibit a similar trend to that of smooth surface caries in terms of the increase in contrast between the treatment window and intact areas as the

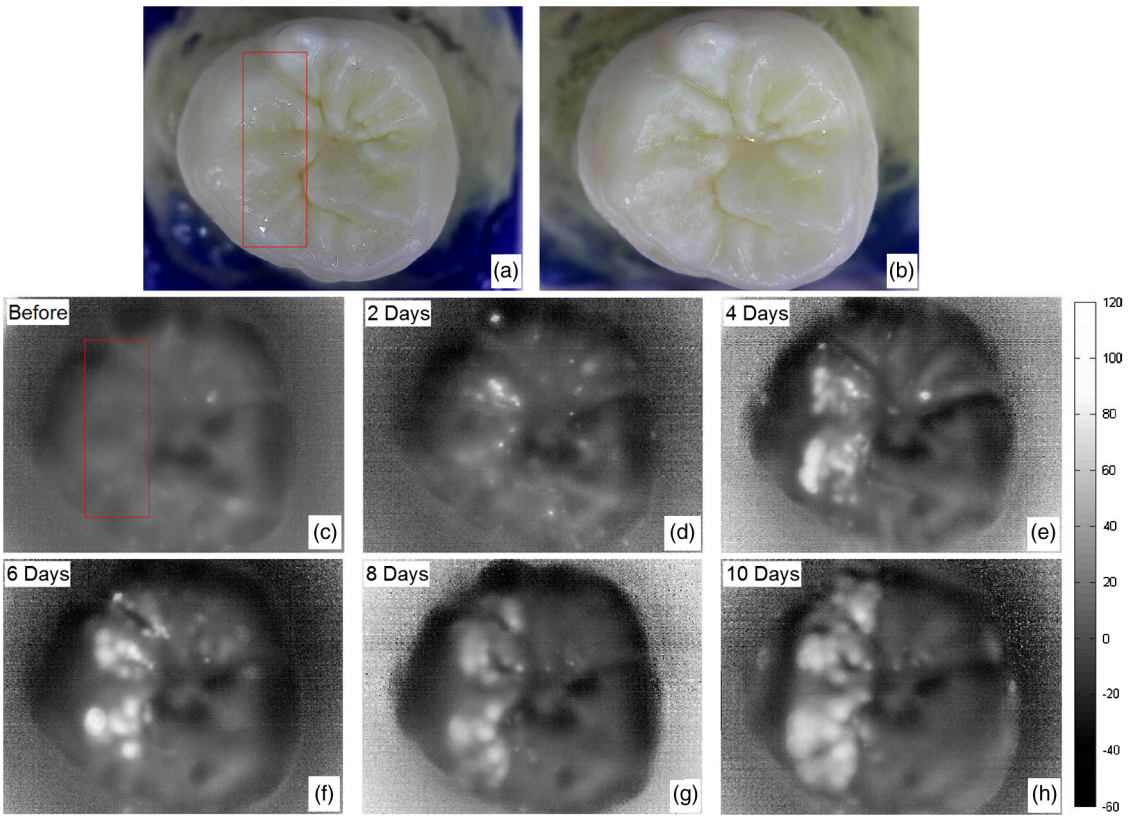

Fig. 5 Optical image of the occlusal surface of extracted human molar (a) before and (b) after 10 days of demineralization on the treatment window. TPLI phase images of sample (c) before and after (d) 2, (e) 4, (f) 6, (g) 8, and (h) 10 days of treatment obtained at 2-Hz modulation frequency.

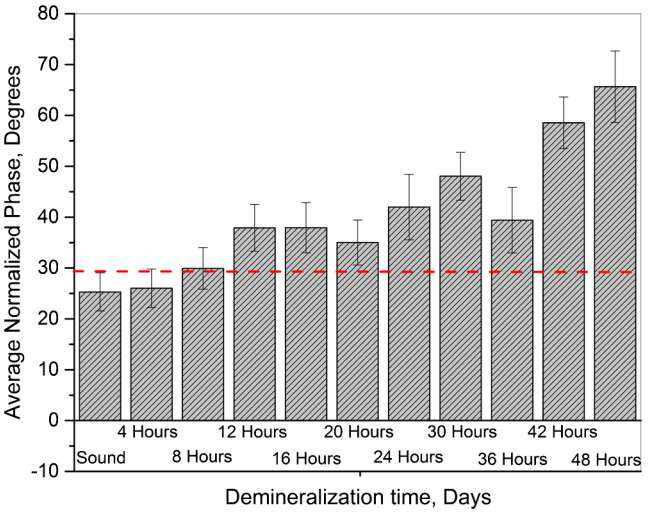

Fig. 6 Average phase values within the treatment window for the sample at several demineralization stages. The dashed line indicates the detection threshold of our low-cost LWIR TPI system.

treatment time increases. However, due to the nonuniformity of physical and structural properties of the occlusal surface and its complex geometry, the extent of demineralization is variable throughout the treatment window.

The obtained results from this study, as the first controlled demineralization imaging investigation on occlusal caries, suggest the potential of the developed LWIR TPLI system in probing early occlusal caries frequently encountered in the clinical practice.

4.3 *Determination of Detection Threshold*

The results obtained from the controlled demineralization studies of smooth surface and occlusal caries indicate that the developed TPLI system using a low-cost LWIR camera is capable of detecting early caries. Another important parameter of a diagnostic modality is its detection threshold (i.e., how early the system can detect caries?). To this end, a time-dependent controlled demineralization procedure is followed in small intervals (4- and 6-h) up to 2 days of treatment to create minute amounts of demineralization in a rectangular window located on the smooth surface of a dental sample. Similar to the previous results, it was observed that as the treatment time increases, the phase contrast between the treatment window and the intact regions increases due to the progression of the artificially induced early caries lesion into the enamel.

The bar plots of Fig. 6 along with their standard deviations suggest that before 12 h of treatment, the system is not sensitive enough to statistically differentiate between the healthy and demineralized tissues as the average phase values of the 4- and 8-h treated windows fall within the standard deviation of phase values obtained from the untreated sample. However, after application of demineralization for 12 h or more, the early caries can be statistically differentiated due to an increase in the average phase values above the detection threshold of the imaging system. The instability in the average phase value trend appears to be consistent with the concurrent occurrence of demineralization and remineralization cycles proposed by the early caries formation mechanism theories.[10]

5 Conclusions

In this study, we present a low-cost thermophotonic lock-in imaging system for detection of early dental caries using an inexpensive LWIR camera. To the best of our knowledge, this work is the first report on the application of active thermography in the LWIR band for diagnostic imaging of biological samples (i.e., detection of early dental caries). Through theoretical modeling, we have demonstrated that thermophotonic detection of early dental caries in the LWIR band results in improvement in the detection sensitivity compared to the previously reported system detecting in the MIR band. The diagnostic performance of the LWIR system has been examined by monitoring the formation and progression of artificially induced early smooth surface and occlusal dental caries. The follow-up *in vitro* experiments confirm the sensitivity of our noncontact and noninvasive diagnostic imaging system to early demineralization, not detectable through conventional clinical inspection methods. The obtained results also suggest that LWIR TPLI is able to effectively probe the occlusal surface of tooth, which cannot be directly imaged through x-ray radiography. Our detection threshold study suggests that the developed system is capable of detecting artificially induced caries of greater than 12 h. In conclusion, the developed low-cost imaging system is able to provide reasonable contrast and sensitivity to early caries lesions and, therefore, has great potential for integration into a commercially and clinically viable dental diagnostic imaging device.

Acknowledgments

We are grateful to the Natural Sciences and Engineering Research Council of Canada for the Discovery Grant awarded to N. T. and to the Lassonde School of Engineering and the York University for their financial support through the institutional start-up grant.

References

1. J. D. Bader, D. A. Shugars, and A. J. Bonito, "A systematic review of the performance of methods for identifying carious lesions," *J. Public Health Dent.* **62**(4), 201–213 (2002).
2. D. Fried et al., "Near-IR imaging of interproximal lesions from occlusal surfaces and the influence of stains and plaque," *Proc. SPIE* **6137**, 61370N (2006).
3. C. Zakian, I. Pretty, and R. Ellwood, "Near-infared hyperspectral imaging of teeth for dental caries detection," *J. Biomed. Opt.* **14**(6), 064047 (2009).
4. C. Meller et al., "A new in vivo method for measuring caries activity using quantitative light-induced fluorescence," *Caries Res.* **40**(2), 90–96 (2006).
5. C. John and A. Salerno, "Raw data set of thermal wave propagation in hard dental tissues," in *Proc. 11th Int. Symp. Computer Assisted Radiology*, Vol. 986, pp. 986–1052 (1997).
6. C. John et al., *Nondestructive Characterization of Materials VIII*, pp. 757–762, Springer, New York (1998).
7. R. J. Jeon et al., "Nonintrusive, noncontacting frequency-domain photothermal radiometry and luminescence depth profilometry of carious and artificial subsurface lesions in human teeth," *J. Biomed. Opt.* **9**(4), 804–819 (2004).
8. D. Fried et al., "Imaging caries lesions and lesion progression with polarization sensitive optical coherence tomography," *J. Biomed. Opt.* **7**(4), 618–627 (2002).
9. N. Tabatabaei, A. Mandelis, and B. T. Amaechi, "Thermophotonic lock-in imaging of early demineralized and carious lesions in human teeth," *J. Biomed. Opt.* **16**(7), 071402 (2011).
10. O. Fejerskov and E. A. M. Kidd, *Dental Caries*, Blackwell Munksgaard, Copenhagen (2003).

11. J. D. Featherstone, "Prevention and reversal of dental caries: role of low level fluoride," *Commun. Dent. Oral Epidemiol.* **27**(1), 31–40 (1999).
12. S. C. White and M. J. Pharoah, *Oral Radiology: Principles and Interpretation*, Elsevier Health Sciences, Philadelphia (2014).
13. J. D. Featherstone and D. Fried, "Fundamental interactions of lasers with dental hard tissues," *Med. Laser Appl.* **16**(3), 181–194 (2001).
14. A. Hall and J. M. Girkin, "A review of potential new diagnostic modalities for caries lesions," *J. Dent. Res.* **83**(1), C89–C94 (2004).
15. B. T. Amaechi, "Emerging technologies for diagnosis of dental caries: the road so far," *J. Appl. Phys.* **105**(10), 102047 (2009).
16. S. Kaiplavil and A. Mandelis, "Truncated-correlation photothermal coherence tomography for deep subsurface analysis," *Nat. Photonics* **8**(8), 635–642 (2014).
17. A. Matvienko et al., "Theoretical analysis of coupled diffuse-photon-density and thermal-wave field depth profiles photothermally generated in layered turbid dental structures," *J. Appl. Phys.* **105**(10), 102022 (2009).
18. N. Tabatabaei, A. Mandelis, and B. T. Amaechi, "Thermophotonic radar imaging: an emissivity-normalized modality with advantages over phase lock-in thermography," *Appl. Phys. Lett.* **98**(16), 163706 (2011).
19. N. Tabatabaei et al., "On the sensitivity of thermophotonic lock-in imaging and polarized Raman spectroscopy to early dental caries diagnosis," *J. Biomed. Opt.* **17**(2), 025002 (2012).
20. N. Tabatabaei and A. Mandelis, "Thermal coherence tomography using match filter binary phase coded diffusion waves," *Phys. Rev. Lett.* **107**(16), 165901 (2011).
21. C. Meola and G. M. Carlomagno, *Nondestructive Testing of Materials and Structures*, pp. 91–96, Springer, The Netherlands (2013).
22. G. Giorleo, C. Meola, and A. Squillace, "The use of lock-in thermography in industrial applications," *Nondestructive Testing Evaluation* **16**(1), 15–29 (2000).
23. Y. K. An, J. M. Kim, and H. Sohn, "Laser lock-in thermography for detection of surface-breaking fatigue cracks on uncoated steel structures," *NDT & E Int.* **65**, 54–63 (2014).
24. M. Rossi et al., *Residual Stress, Thermomechanics & Infrared Imaging, Hybrid Techniques and Inverse Problems*, Vol. **8**, pp. 207–213, Springer, New York (2013).
25. A. Ojaghi, A. Parkhimchyk, and N. Tabatabaei, "A pilot study on the detection of early proximal and occlusal dental caries using long-wave infrared thermophotonic imaging," *Proc. SPIE* **9692**, 969209 (2016).
26. A. Mandelis, *Diffusion-Wave Fields: Mathematical Methods and Green Functions*, Springer, New York (2013).
27. O. Breitenstein and M. Langenkamp, *Lock-in Thermography: Basics and Use for Functional Diagnostics of Electronic Components*, Springer, New York (2003).
28. B. T. Amaechi, S. M. Higham, and W. M. Edgar, "Factors affecting the development of carious lesions in bovine teeth in vitro," *Arch. Oral Biol.* **43**(8), 619–628 (1998).
29. A. Hellen et al., "Quantitative evaluation of the kinetics of human enamel simulated caries using photothermal radiometry and modulated luminescence," *J. Biomed. Opt.* **16**(7), 071406 (2011).
30. A. Hellen, A. Mandelis, and Y. Finer, "Photothermal radiometry and modulated luminescence examination of demineralized and remineralized dental lesions," *J. Phys. Conf. Ser.* **214**(1), 012024 (2010).
31. R. J. Jeon et al., "Experimental investigation of demineralization and remineralization of human teeth using infrared photothermal radiometry and modulated luminescence," *Proc. SPIE* **6856**, 68560B (2008).
32. A. Hellen et al., "Optothermophysical properties of demineralized human dental enamel determined using photothermally generated diffuse photon density and thermal-wave fields," *Appl. Opt.* **49**(36), 6938–6951 (2010).
33. B. T. Amaechi et al., "Application of optical coherence tomography for imaging and assessment of early dental caries lesions," *Laser Phys.* **13**(5), 703–710 (2003).
34. P. D. Marsh and D. J. Bradshaw, "Dental plaque as a biofilm," *J. Ind. Microbiol.* **15**(3), 169–175 (1995).
35. R. S. Jones and D. Fried, "Attenuation of 1310-and 1550-nm laser light through sound dental enamel," *Proc. SPIE* **4610**, 187 (2002).
36. J. C. Simon et al., "Transillumination and reflectance probes for in vivo near-IR imaging of dental caries," *Proc. SPIE* **8929**, 89290D (2014).
37. D. Fried et al., "Near-IR imaging of interproximal lesions from occlusal surfaces and the influence of stains and plaque," *Proc. SPIE* **6137**, 61370N (2006).
38. E. C. Almaz et al., "Influence of stains on lesion contrast in the pits and fissures of tooth occlusal surfaces from 800-1600-nm," *Proc. SPIE* **9692**, 96920X (2016).
39. C. M. Bühler, P. Ngaotheppitak, and D. Fried, "Imaging of occlusal dental caries (decay) with near-IR light at 1310-nm," *Opt. Express* **13**(2), 573–582 (2005).

Ashkan Ojaghi is a master's student in the Department of Mechanical Engineering at York University (Canada). He received his BSc degree in mechanical engineering from the Iran University of Science and Technology in 2014. He joined the Hybrid Biomedical Optics Laboratory at York University in September 2014 and is currently conducting research on long-wave infrared thermophotonic imaging of demineralization in hard dental tissues.

Artur Parkhimchyk: Biography is not available.

Nima Tabatabaei is an assistant professor in the Department of Mechanical Engineering and the director of Hybrid Biomedical Optics Laboratory (www.HBOLab.ca) at York University (Canada). He received his PhD in mechanical engineering from the University of Toronto in 2012 and conducted postdoctoral research at Harvard Medical School 2012 to 2014. His research interests are design and development of hybrid biomedical optics imaging technologies for early diagnosis of soft and hard tissue diseases.